J Vis (2010) 13:141–149
DOI 10.1007/s12650-009-0020-7

REGULAR PAPER

Trushar B. Gohil · Arun K. Saha · K. Muralidhar

Control of flow in forced jets: a comparison of round and square cross sections

Received: 14 May 2009 / Accepted: 17 November 2009 / Published online: 8 January 2010

Abstract Direct numerical simulation of incompressible, spatially developing round and square jets at a Reynolds number of 1,000 is performed. The effect of two types of inlet perturbation on the flow structures is analyzed. First, dual-mode excitation, which is a combination of axisymmetric perturbation at preferred mode frequency and helical perturbation at sub-harmonic frequency is used, having a disturbance frequency ratio equal to $R_f = 2$. It is observed that the circular and square jets bifurcate and spread on one of the orthogonal planes forming a Y-shape jet in the downstream while no spreading is visible on the other plane. The second type of perturbation is a flapping excitation at a sub-harmonic frequency, $St_F = 0.2$. It leads to a Y-shape bifurcation for both square and circular jets. On the other hand, for flapping excitation at the preferred mode frequency, namely, $St_F = 0.4$, a circular jet bifurcates into a Ψ-shape whereas the square jet reveals simple spreading.

Keywords Jet control · Round jets · Square jets · DNS · Bifurcating jets

List of symbols

D	Nozzle diameter
A_a, A_h, A_f	Amplitude of axial, helical and flapping excitation, respectively
Re_D	Jet Reynolds number, $U_{inlet}D/v$
p	Pressure
S_{ij}	Strain rate tensor, $\left(u_{i,j} + u_{j,i}\right)/2$
St_D, St_H, St_F	Strouhal number for axial, helical and flapping perturbation respectively, $St = fD/U_{inlet}$
t	Time
$u_i^{noise}(r, t)$	Noise (velocity) in $i = x, y$ and z directions
$u_x^{forced}(r, t)$	Large-scale perturbation
u_x, u_y, u_z	Velocity in x, y and z directions
U_{inlet}	Maximum inlet velocity
x, y, z	Cartesian coordinates

List of Greek symbols

Ω_{ij}	Rotational tensor, $\left(u_{i,j} - u_{j,i}\right)/2$
θ_m	Inlet momentum thickness, $\int_0^{D/2} \bar{u}/U_{inlet}(1 - \bar{u}/U_{inlet})r\mathrm{d}r$
θ_c	Azimuthal direction in cylindrical coordinate
v	Kinematic viscosity

T. B. Gohil · A. K. Saha (✉) · K. Muralidhar
Department of Mechanical Engineering, Indian Institute of Technology Kanpur, Kanpur 208016, India
E-mail: aksaha@iitk.ac.in

1 Introduction

Free jets are important in several industrial applications such as combustion, propulsion, mixing, and aeroacoustics. Jet control leading to noise reduction and efficient combustion can be achieved by manipulating the coherent structure that is formed near the exit plane.

At low Reynolds number and noise-free conditions, the flow field of a jet reaches a well-defined steady state. For naturally evolving homogeneous free jets at relatively higher Reynolds number, a thin shear layer is formed at the nozzle exit. The shear layer is subjected to Kelvin–Helmoltz (KH) instability and produces vortex rings. These ring structures become larger by successive pairing. In the downstream direction, subsequent tearing due to nonlinear interactions results in the appearance of complex fine-scale structures. Streamwise rib vortices develop in the braid region between primary structures and these vortices are responsible for the creation of small scales outside the potential core. The presence of small-scale fluctuations at the exit of the nozzle also leads to early transition from both the steady and unsteady jets leading to KH ring vortices all the way to complex structures with multiple length scales. The scale distribution depends on both Reynolds number and the streamwise location.

Numerical simulation of transitional and turbulent flows requires sufficient computer resources and a high-order numerical algorithm. With the availability of high-speed computers and development of algorithms of high accuracy, it is possible to study spatial jets by means of direct numerical simulation (DNS). At the same time free transitional turbulent flows, similar to that studied in the present work, are more difficult to simulate as compared to internal flows because of the absence of a clear boundary. Here, spatial development is a result of entrainment of the ambient fluid into the jet region and should be obtained as a part of the overall solution.

Lee and Reynolds (1985) and Parekh et al. (1988) showed that it is possible to make a round jet bifurcate by simultaneously imposing helical and axial modes of forcing. The requisite condition for bifurcation is helical forcing having a frequency equal to twice the axial forcing frequency. Danaila and Boersma (1998), (2000) investigated the mechanism of bifurcation with the aid of DNS. The authors imposed an oscillating component consisting of a pair of counter-rotating helical modes on the nozzle exit velocity and showed that the single-frequency excitation could trigger bifurcation of the jet. da Silva and Metais (2002) studied flapping excitation at preferred and sub-harmonic modes for various Reynolds numbers. They concluded that the maximum spreading rate is achieved by applying a sub-harmonic frequency. Suzuki et al. (2004) developed a miniature electromagnetic flap actuator and mount on the nozzle exit of an axisymmetric jet and experiments are conducted at $St_D = 0.25$ and $2{,}000 < Re_D < 13{,}000$. The authors demonstrated that flap actuators can significantly modify the large-scale coherent structures.

In the present study, DNS of free circular and square jets has been performed for two types of forcing, namely, flapping and dual-mode excitation. The impact of various forcing functions at the nozzle exit has been studied with respect to the jet structure and the spreading rate. Y- and Ψ-shaped bifurcation phenomena are observed depending on the inlet perturbation.

2 Numerical methodology

2.1 Governing equations

In the present study, simulation is performed by solving the three-dimensional, unsteady, incompressible Navier–Stokes equations written as:

$$\frac{\partial u_i}{\partial x_i} = 0 \tag{1}$$

$$\frac{\partial u_i}{\partial t} + \frac{\partial \left(u_i u_j\right)}{\partial x_j} = -\frac{\partial p}{\partial x_i} + \frac{1}{\mathrm{Re}_D}\frac{\partial^2 u_i}{\partial x_j^2}. \tag{2}$$

Equations 1 and 2 are non-dimensionalized using length scale D (nozzle exit size) and velocity scale U_{inlet} (maximum inlet velocity), while time and pressure are non-dimensionalized by D/U_{inlet} and ρU_{inlet}^2, respectively. Reynolds number for the present work is defined as $Re_D = U_{\text{inlet}}D/\nu$, ν being the kinematic viscosity.

The solution algorithm is based on MAC (Marker and cell) formulation proposed by Harlow and Welch (1966). Temporally, second-order Adams–Bashforth scheme is employed for the convective terms while the diffusion terms is discretized using a Crank–Nicolson scheme. With this approach, the viscous stability constraint is eliminated and increases the flexibility in the choice of the time step. The pressure Poisson equation is solved using a Gauss–Seidel over-relaxation method. The equations are discretized on a staggered grid in which velocity vector is defined at the all faces while pressure is defined at the cell center. The convective terms are discretized spatially using a weighted averaged fourth-order central difference and fifth-order upwind-biased schemes and diffusion terms are discretized using a fourth-order central-difference scheme.

2.2 Boundary conditions

On the inlet boundary, velocity profile is prescribed as an inlet condition at each time step and is given by

$$\begin{aligned} u_x^{\text{inlet}}(r,t) &= u_x^{\text{profile}}(r) + u_x^{\text{noise}}(r,t) + u_x^{\text{forced}}(r,t) \\ u_y^{\text{inlet}}(r,t) &= u_y^{\text{noise}}(r,t) \\ u_z^{\text{inlet}}(r,t) &= u_z^{\text{noise}}(r,t). \end{aligned} \tag{3}$$

Here $u_i^{\text{inlet}}(r, t)$ is the instantaneous inlet velocity vector and $r = \sqrt{y^2 + z^2}$. The expression for $u_x^{\text{profile}}(r)$ is given by Eq. 4 while $u_i^{\text{noise}}(r, t)$and $u_x^{\text{forced}}(r, t)$ are three components of random and large-scale perturbations respectively. In above equations, subscript i can take any value among x, y, and z depending on the direction of velocity component.

The time-averaged streamwise velocity variation given by Michalke and Hermann (1982) is used at the inflow plane. It is known to be a good approximation of the measured velocity profiles in round jets at a location which is little away from the jet exit. The modeled streamwise velocity is given as

$$u_x^{\text{profile}}(r) = \frac{(U_{\text{inlet}})}{2}\left\{1 + \tan h\left[\frac{R-r}{2\theta_{\text{m}}}\right]\right\}. \tag{4}$$

The inlet velocity profile for square jets has also been generated using Eq. 4 though suitable adjustments are required to be carried out. In Eq. 4, U_{inlet} is the maximum inlet velocity and θ_{m} is the momentum thickness of the shear layer at inlet. Figure 1a shows velocity profiles for both circular and square jets.

At the inlet, the two components of the time-averaged transverse velocity are set to zero. Both random and large-scale perturbations with zero time-averaged values are superimposed on the inlet velocity variation described by Eq. 4. A white noise signal $u_i^{\text{noise}}(r, t)$ that has amplitude of 5% of the rms fluctuation is

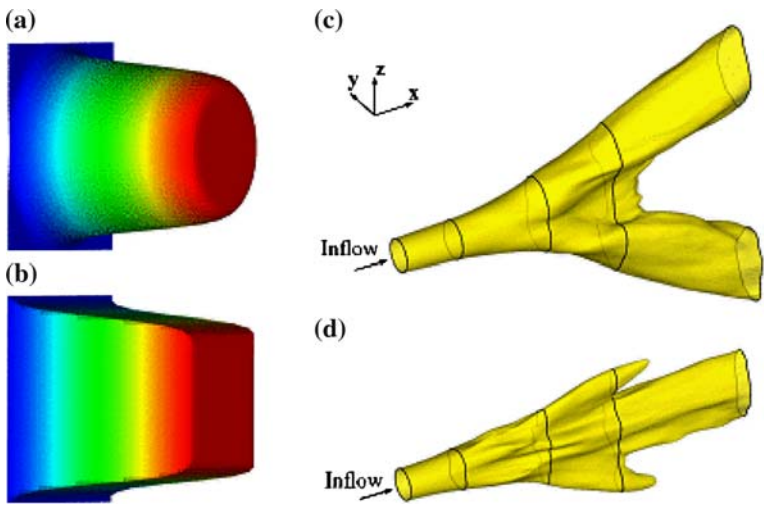

Fig. 1 Representative inlet velocity profiles for circular (**a**) and square (**b**) jets. Schematic drawing of Y-shape (**c**) and Ψ-shape (**d**) bifurcating jets in the form of isosurfaces of time-averaged axial velocity

added to all the three velocity components even for the natural unforced jet. The various type of large-scale perturbation $u_x^{\text{forced}}(r, t)$ used in the present study for controlling jets are discussed below.

It is to be mentioned that the white noise has little effect on flow structures at Reynolds number of the current study, i.e., $Re = 1{,}000$. In the present study, the focus is on the influence of large-scale perturbations, white noise effects being small. At $Re = 2{,}000$, white noise had a stronger role and is a topic of future research.

2.2.1 Dual-mode excitation (DME)

In the present study, DME perturbation is obtained by combining an axisymmetric excitation at the preferred mode frequency and helical excitation at a frequency fixed by the disturbance frequency ratio $R_f = St_D/St_{\text{H}}$ where St_D and St_{H} are the axial and helical excitation Strouhal numbers, respectively. The expression for the DME excitation in the present study is given as

$$u_x^{\text{forced}}(r,t) = \left\{ A_{\text{a}} u_x^{\text{profile}}(r) \sin\left(2\pi St_D \frac{U_{\text{inlet}}}{D} t\right) \right\} + \left\{ A_{\text{h}} u_x^{\text{profile}}(r) \sin\left(2\pi St_{\text{H}} \frac{U_{\text{inlet}}}{D} t - \theta_{\text{c}}\right) \left(\frac{2r}{D}\right) \right\}.$$

The amplitude of imposed excitation is $A_{\text{a}} = A_{\text{h}} = 15\%$ of the peak fluctuation and θ_{c} is the azimuthal direction in cylindrical coordinate.

2.2.2 Flapping excitation (FLE)

The formula for flapping excitation is taken as:

$$u_x^{\text{forced}}(r,t) = A_{\text{f}} u_x^{\text{base}}(r) \sin\left(2\pi St_{\text{F}} \frac{U_{\text{inlet}}}{D} t\right) \sin\left(\frac{2\pi y}{D}\right).$$

Here A_{f} is the amplitude of the imposed excitation and is set to a value of 15% of the peak fluctuation; y is one of the transverse directions and St_{F}, the flapping excitation Strouhal number. In the above expression $u_x^{\text{base}}(r)$ is given as

$$u_x^{\text{base}}(r) = \begin{cases} 1 & \text{if } 0.4 < r/D < 0.6 \\ 0.2 & \text{if } r/D < 0.4 \\ 0 & \text{otherwise} \end{cases}.$$

Unlike white noise, the large-scale perturbation has been applied only to the streamwise velocity component.

A non-reflective outflow condition developed by Orlanski (1976) is used at the outflow boundary. Both transverse confining surfaces are modeled as periodic boundaries. The domain size (Fig. 1b) adopted for simulation in the x, y, and z directions is $12 \times 10.65 \times 10.65$ and the corresponding grid sizes are $210 \times 192 \times 192$. The mesh is uniform in the streamwise direction while in both transverse directions, a non-uniform mesh is used. Reynolds number based on the jet dimension and maximum inlet velocity U_{inlet} is 1,000 and the ratio of the jet radius to initial shear layer momentum thickness is fixed at $R/\theta = 20$.

A grid sensitivity test has been undertaken at a Reynolds number of 1,000 on four different grid sizes namely, $160 \times 144 \times 144$, $210 \times 192 \times 192$, $290 \times 264 \times 264$ and $320 \times 384 \times 384$ for the circular jet with a small-scale perturbation of 5%. A comparison of the decay of the time-averaged axial velocity along the centerline and the time-averaged streamwise velocity profile at a downstream location $x/D = 10.0$ shows no difference between the last three grid sizes (Fig. 2). Therefore, a grid resolution of $210 \times 192 \times 192$ is considered adequate and is utilized for all the simulations reported in the present study. It is to be mentioned that FFTs of velocity signals computed using all the grids mentioned above at far downstream suggest that the flow is not fully turbulent, in the sense of attaining the $-5/3$ slope in the dissipation range, within the domain of the present study.

3 Results and discussion

Large-scale coherent structures in turbulent shear flow play a primary role in transport phenomena and selective manipulation of these structures is desired in orders to achieve an efficient control. In the present

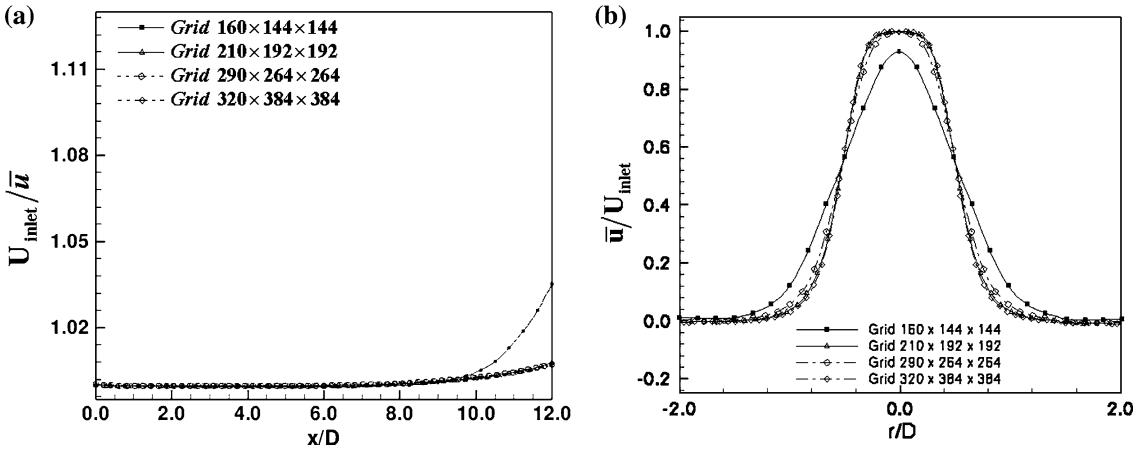

Fig. 2 **a** Decay of time-averaged axial velocity on the centerline and **b** time-averaged axial velocity profiles at $x/D = 10$ and $Re = 1{,}000$ with 5% white noise

Table 1 Description of parameters for various simulations

Simulation	Type of nozzle	Forcing type	St_D or St_F	St_H	R_f
CNLR	Circular	Natural	–	–	–
CDME_2.0	Circular	Combined axial and helical	0.4	0.2	2.0
SDME_2.0	Square	Combined axial and helical	0.4	0.2	2.0
CFLE_0.2	Circular	Flapping	0.2	–	–
SFLE_0.2	Square	Flapping	0.2	–	–
CFLE_0.4	Circular	Flapping	0.4	–	–
SFLE_0.4	Square	Flapping	0.4	–	–

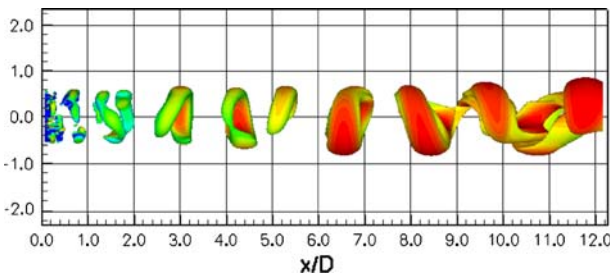

Fig. 3 Isosurfaces of vortical structures for a circular natural jet (CNLR). Chosen threshold is $0.05(U_{inlet}/D)2$ and colored by vorticity modulus varying between 0.1 (*red*) to 2 (*blue*). Of interest is the transformation of a circular vortex ring towards a helical structure

study two different types of inlet perturbation, namely, dual-mode and flapping are designed for control of the jet. Table 1 summarizes the cases considered and the corresponding parameters.

For a circular natural jet (CNLR), well-defined vortex rings are shed at the preferred mode frequency. The appearance of a KH ring in the vortical structures (Fig. 3) is quite clear around $x/D = 3$. The *Q-criterion* which deals with the second invariant of velocity gradient tensor (Hunt et al. 1988) is used to extract the vortical structures from the simulation data. Here, Q is given as $Q = 1/2\left(\Omega_{ij}\Omega_{ij} - S_{ij}S_{ij}\right)$. Further, $\Omega_{ij} = \left(u_{i,j} - u_{j,i}\right)/2$ is the anti-symmetric and $S_{ij} = \left(u_{i,j} + u_{j,i}\right)/2$ the symmetric part of the velocity gradient tensor $\nabla\vec{u}$. Positive Q isosurfaces isolate areas where the strength of rotation overcomes strain, thus making those surfaces eligible as vortex envelopes. Since vorticity should increase as the center of the vortex is approached, Q can be expected to remain positive in the core of the vortex. The positive Q regions are good indicators of the coherent vortices in various wall-bounded or free-shear flows.

The vortex rings of Fig. 3 become progressively inclined, the angle of which increases with the downstream distance. Around $x/D = 8.5$, a helix-like structure is visible in the flow, which suggest, the emergence of helical mode. This is consistent with stability analysis which predicts the helical mode of azimuthal wave number to be the most unstable for $R/\theta < 6.5$ (da Silva and Metais 2002). For the present investigation, the transition distance is about $x/D \sim 9$. For $Re_D = 1{,}500$ (da Silva and Metais 2002) also show similar structures for natural jets at a location $x/D \sim 10$. Fast Fourier transform of the axial velocity signal at $x/D = 4.07$ shows the dominant frequency to be 0.4 in terms of St_D. The calculated frequency of the preferred mode is found to lie within the range (0.24–0.64) as cited in previous studies (Ephrain and Ho 1983). The preferred mode frequency found from the simulation of a natural jet is used as one of the forcing modes for perturbing the jet.

The second mode of excitation is sub-harmonic and is equal to 0.2 in the present study. The growth of the sub-harmonic mode is associated with alternate pairing arrangement of the vortex rings. As discussed earlier, these two modes (preferred and sub-harmonic) are used to design two types of inlet perturbation, namely, dual-mode and flapping mode excitations. For generating dual-mode excitation, an axial excitation is applied at the preferred mode frequency and a helical excitation has been applied at the sub-harmonic mode frequency. For flapping excitation, St_F is chosen to be either preferred or sub-harmonic mode frequency. The designed inlet perturbation is applied to two different types of nozzles of circular and square cross sections.

The influence of different types of forcing on the evolution of vortical structure is revealed through the instantaneous flow field. Figure 4 shows two orthogonal views of isosurfaces of vortical structures for circular and square jets. The transition of KH ring vortices to complex small-scale structures is clearly discerned. In circular jets, the main mechanism leading to the shear layer growth is vortex interaction and merging. However, the generation of small-scale structure is attributed to vortex tearing resulting from the

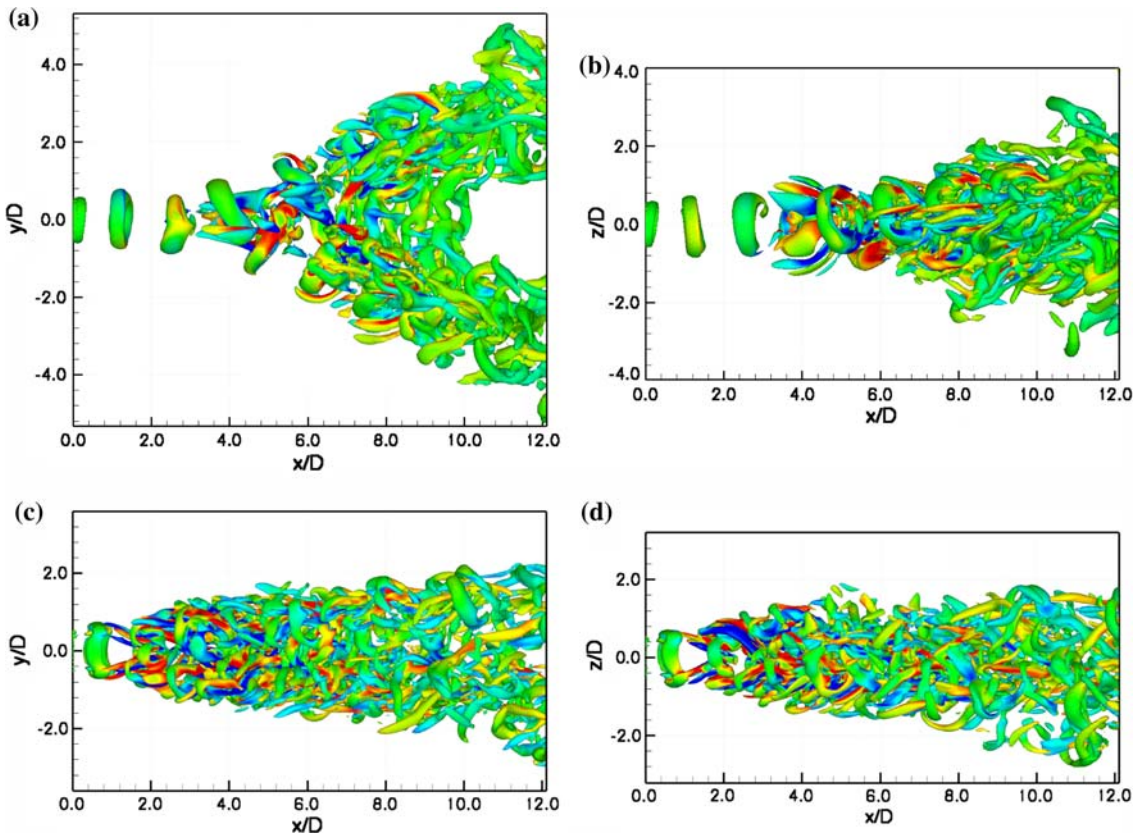

Fig. 4 Isosurfaces of vortical structures in two orthogonal views for jets with dual-mode excitation; chosen threshold is $0.1(U_{inlet}/D)2$ and figures are *colored* by the streamwise vorticity. With reference to Table 1, **a** and **b** (*top row*) represent CDME_2.0 while **c** and **d** (*lower row*) are for SDME_2.0. In the *x*–*y* plane, both jets have a clear Y-shape bifurcation

intense interaction among vortices. In contrast, in case of square jets the dynamics of self-induced vortex deformation appears to be more important than the vortex merging process for the shear layer growth.

For a circular jet, the circular vortex sheet rolls up into vortex rings due to KH instability and subsequently they interact with each other leading to small-scale structures. In a square jet, the square vortex sheet rolls up into square vortex rings near the inflow, and due to self-induction the corner region moves ahead, faster than the other portion of the ring. Consequently, rib vortices are generated that align themselves along the corner of the square ring as is apparent in Fig. 4c.

The first important observation from Fig. 4 is the spectacular increase of jet spreading on one of the orthogonal planes while it is not significant on the other plane. It is also interesting to note that the square jet suffers from early transition compared to the circular jet, though both are subject to similar dual-mode perturbations. Dual-mode excitation causes both circular as well as square jets to split into two separate jets on the bifurcating plane. The angle between the two separated jets is greater for circular jets than that of the square jet. The smaller spreading for a square jet is due to the formation of a pair of rib vortices at the corner of the jets.

In case of flapping excitation, two alternating inclined vortex rings are shed within a time period, the frequency of which is $2St_F$. The difference as compared to axisymmetric excitation, for example, an axial perturbation is the following: one vortex is generated in one half of the cycle while the other one shows up in the other half of the cycle whose orientation is dictated by the inlet perturbation. The non-uniformity in the streamwise velocity makes the vortical structures tilted. It is to be noted that the streamwise location where the interaction between two successive vortices starts strongly depends on the frequency of perturbation and diffusion of vortices.

Flapping excitation at the sub-harmonic frequency $St_F = 0.2$, when applied to circular and square jets (Fig. 5), lead to the bifurcation of the main jet to two smaller separate jets. Though the instantaneous vortical structures in a square jet (Fig. 5c) do not show distinct bifurcation within the streamwise extent of

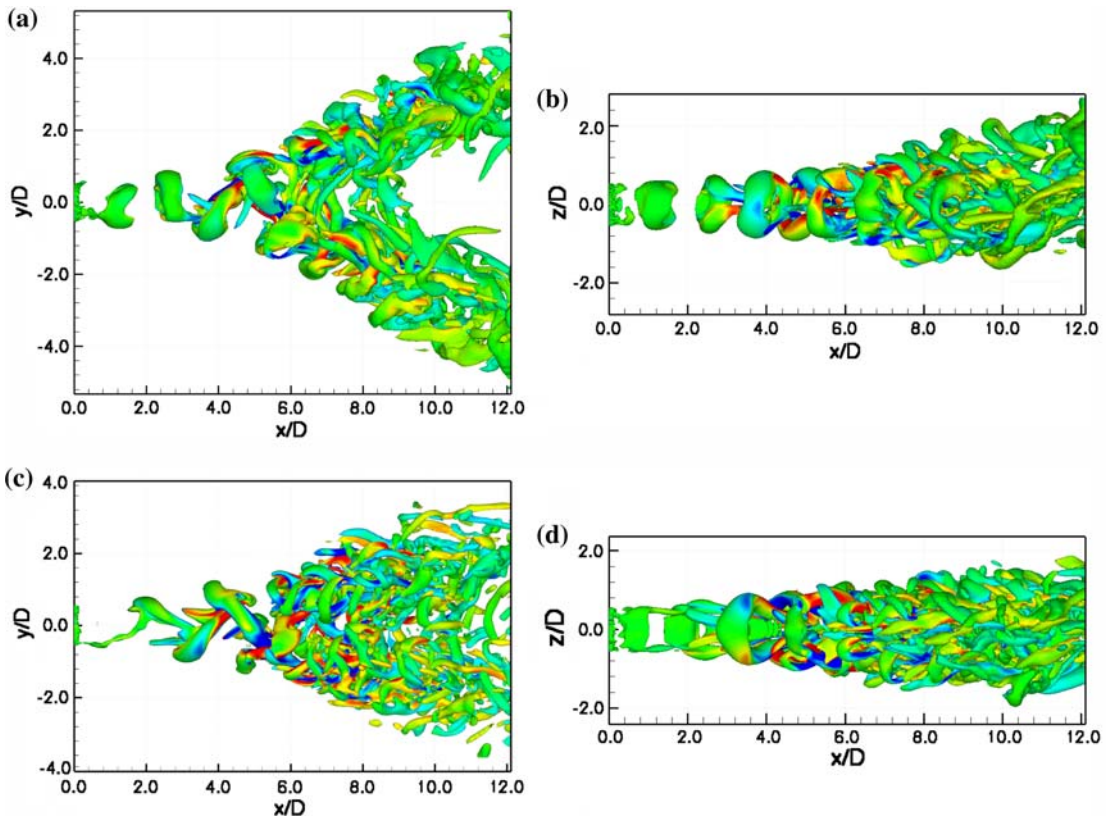

Fig. 5 Isosurfaces of vortical structures in a two orthogonal view for jets driven by the flapping excitation; legend as in Fig. 4. With reference to Table 1, **a** and **b** (*top row*) represent CFLE_0.2 while **c** and **d** (*lower row*) are for SFLE_0.2. In the *x*–*y* plane, the Y-shaped bifurcation for the circular jet is quite distinct, while it is somewhat weak for the square jet within the domain of present computations

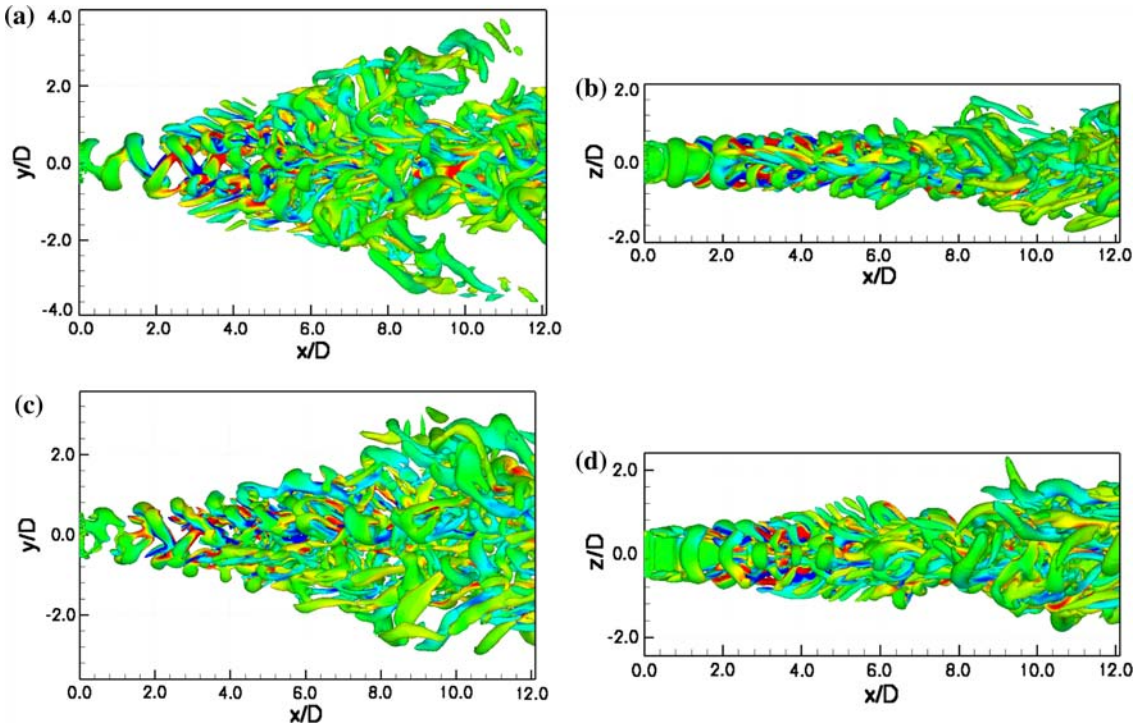

Fig. 6 Isosurfaces of vortical structures in a two orthogonal views for jets driven by flapping excitation; legend as in Fig. 4. *Top row* (**a** and **b**) represents CFLE_0.4 while **c** and **d** (*lower row*) are for SFLE_0.4. The circular jet has a Ψ-shaped bifurcation while the square jet does not show any evidence of Ψ-shaped bifurcation within the domain of the present computation

the present study as it seen in circular jet (Fig. 5a), the time-averaged field (not shown here) of square jet reveals clear bifurcation. On the other hand, for the preferred mode frequency of $St_F = 0.4$, the circular jet shows a bifurcation nature which is quite different from that at $St_F = 0.2$ (Fig. 6a, b). The spread in Fig. 6a depicts a Ψ-shape. However, the square jet (Fig. 6c, d) does not show any evidence of Ψ-shape bifurcation especially within the domain of the present computations. Da Silva and Metais (2002) studied flapping excitation at both sub-harmonic and preferred mode frequency for Reynolds numbers ranging from $Re_D = 1.5 \times 10^3$–5.0×10^4 and reported only spreading without any bifurcation.

Danaila and Boersma (1998, 2000) studied both flapping and dual-mode excitation for circular jets at $Re_D = 1{,}500$ and $R/\theta = 30$. For flapping excitation at a sub-harmonic frequency, the authors also reported Y-shape bifurcation, but for dual-mode excitation their result revealed a Ψ-shape bifurcation. However, the present study shows a Y-shape bifurcation for dual-mode as well as for flapping excitation at a sub-harmonic frequency and Ψ-shape bifurcation for flapping excitation at the preferred mode frequency. The probable reason for getting the Ψ-shaped bifurcation in Danaila and Boersma (1998, 2000) could be because dual-mode excitation was generated in their study using counter-rotating helical modes. The present work employs unidirectional dual-mode excitation. Suzuki et al. (2004) also studied the flapping excitation at $St_D = 0.25$ and $2{,}000 < Re_D < 13{,}000$. They also observed the bifurcation of the jet; however, since a square wave signal was employed for excitation, the formation mechanism of the tilted vortices is different from the present study. Spreading of square jets by various types of excitation is less when compared to circular jets. The lower spreading is due to the presence of rib vortices at the corners. Square jets bifurcate with greater difficulty as compared to circular jets when both are subject to a given type of inlet perturbation. The present study uniquely captures bifurcation of a forced square jet by a large-scale perturbation.

4 Conclusions

The evolution of round and square jets at a Reynolds number of 1,000 under dual-mode and flapping excitation is examined using DNS. In circular jets, the main mechanism leading to the shear layer growth

and formation of small-scale structure is vortex interaction and merging. In contrast, in case of square jets the dynamics of self-induced vortex deformation mechanism is more important. Dual-mode excitation leads both jets to bifurcate into two separate jets at $R_f = 2$. For flapping excitation at sub-harmonic frequency, both jets show Y-shape bifurcation. However at preferred mode frequency, circular jet shows Ψ-shape bifurcation while square jet has only spreading. Circular jet has a larger angle of bifurcation as compared to the square jet.

References

da Silva CB, Metais O (2002) Vortex control of bifurcating jets: a numerical study. Phys Fluids 14:3798
Danaila I, Boersma BJ (1998) Mode interaction in a forced homogeneous jet at low Reynolds numbers. In: Proceeding of the summer program. CTR, pp 141–158
Danaila I, Boersma BJ (2000) Direct numerical simulation of bifurcating jets. Phys Fluids 12:1255–1257
Ephrain G, Ho C-M (1983) Preferred modes and the spreading rates of jets. Phys Fluids 26:2932
Harlow FH, Welch JE (1966) Numerical study of large- amplitude free-surface motions. Phys Fluids 9:842
Hunt JCR, Wray AA, Moin P (1988) Eddies, stream, and convergence zones in turbulent flows. Report CTR-S88, Center for Turbulence Research
Lee M, Reynolds WC (1985) Bifurcating and blooming jets. Report TF-22, Thermosciences Division, Department of Mechanical Engineering, Stanford University, Stanford, CA
Michalke A, Hermann G (1982) On the inviscid instability of a circular jets with external flow. J Fluid Mesh 114:343
Orlanski I (1976) A simple boundary condition for unbounded flows. J Comput Phys 21:251–269
Parekh DE, Leonard A, Reynolds WC (1988) Bifurcating jets at high Reynolds numbers. Report TF-35, Thermosciences Division, Department of Mechanical Engineering, Stanford University, Stanford, CA
Suzuki H, Kasagi N, Suzuki Y (2004) Active control of an axisymmetric jet with distributed electromagnetic flap actuators. Exp Fluids 36:498–509